Global particle-in-cell simulations of microturbulence with kinetic electrons[a)]

J. L. V. Lewandowski[b)]
Princeton University, Princeton Plasma Physics Laboratory, P.O. Box 451, Princeton, New Jersey 08543

G. Rewoldt, S. Ethier, and W. W. Lee
Princeton University, Princeton Plasma Physics Laboratory, P.O. Box 451, Princeton, New Jersey 08543

Z. Lin
Physics and Astronomy, University of California, Irvine, California 92697

(Received 21 October 2005; accepted 29 November 2005; published online 21 July 2006)

The effects of nonadiabatic electrons on ion temperature gradient drift instabilities have been studied in global toroidal geometry using the gyrokinetic particle simulation approach. Compared to the nonlinear global simulations based on only the adiabatic response of the electrons, we have found that the cross-field ion heat transport is two to three times larger in the presence of trapped electrons as compared to the purely adiabatic electron case, and that the zonal component of the electrostatic potential has a shorter wavelength. The numerical methods for calculating both the adiabatic and the nonadiabatic responses for the electrons are presented. © *2006 American Institute of Physics*. [DOI: 10.1063/1.2221931]

I. INTRODUCTION

It is now generally accepted in the fusion community that low-frequency, small-scale instabilities [e.g., drift waves, ion temperature gradient-driven (ITG) modes] are major contenders for the anomalous, cross-field transport observed in tokamaks[1] and stellarators.[2] Although there has been a substantial increase in the available computing power over the past decade, global particle-in-cell simulations of turbulent plasmas have until very recently solely focused on ion-temperature gradient turbulence in the presence of adiabatic electrons. However the impact of the kinetic electrons on ITG turbulence in global toroidal systems is the most important topic. One of the reasons why the study of kinetic electrons in global particle-in-cell (PIC) simulations has received little attention is mainly due to a computational difficulty: the electrons, on average, move much faster ($\sim\sqrt{m_i/m_e}$) than the ions, which translates into a small time step of integration in PIC codes. An obvious brute force method to retain electron dynamics in global PIC simulations is to simply increase the number of electron markers and to decrease the time step of integration; however the computational (and accuracy) requirements implied by this approach for *large-scale, global* PIC simulations far exceed the existing available computing resources. Therefore we must devise new *computational* methods, based on physical intuition (and sometimes not!), to make the simulations of electrons in global PIC simulations accessible to existing massively parallel supercomputers.

As mentioned above, the treatment of kinetic electrons in particle-in-cell simulations is made difficult due to the fact that the electrons move much faster than the ions. However, for drift-type modes,[3–10] the bulk of the electrons respond adiabatically to the waves and it may be advantageous to focus on the nonadiabatic part of the electron response. Based on this observation, a new scheme for the treatment of kinetic electrons that captures all the low-frequency phenomena of interest has recently been developed[12] and generalized to include the Boltzmann response for the adiabatic part for completeness.[11] It has been shown in one-dimensional simulations of drift waves that this type of scheme is more accurate than the δf scheme.[11,13] This paper is a generalization of this type of the treatment of the electrons to toroidal geometry and its implementation to the global gyrokinetic code GTC.[28] Using an electrostatic version of the fluid-kinetic hybrid electron model,[22] kinetic electrons have also recently been implemented in GTC.[18] We would like to point out that many new ideas and numerical schemes have recently proposed to include kinetic electron dynamics in PIC simulations in the presence of electromagnetic effects.[20–26,30]

This paper is organized as follows: in Sec. II the extension of the splitting scheme to toroidal geometry is presented; linear benchmarks and preliminary nonlinear results are reported in Sec. III, followed by concluding remarks in Sec. IV.

II. TREATMENT OF NONADIABATIC RESPONSE OF THE ELECTRONS

A. Preliminary remarks

In this section we describe a numerical technique for the treatment of the kinetic electrons in the simulation of microturbulent plasmas in toroidal geometry. The scheme, as stated earlier, is based on physical intuition: essentially the idea is to remove the adiabatic response of the electrons analytically and to resolve the nonadiabatic response numeri-

[a)]This paper is based on an invited paper presented at the annual APS DPP Meeting in Denver, Colorado, October, 2005. Paper KI1 5, Bull. Am. Phys. Soc. **50**, 181 (2005).
[b)]Invited speaker.

cally. One important feature of this type of scheme is that it allows for the suppression of unwanted high-frequency oscillations. The dependence of the thermal fluctuation level on the plasma β (≡kinetic pressure/magnetic pressure) in a gyrokinetic plasma[30] and the presence of strange attractors in electrostatic drift-wave turbulence with kinetic electrons[31] are examples of phenomena that can only be addressed using the scheme. For a one-dimensional model problem the electron probability distribution function (PDF), in terms of the Boltzmann response can be written as

$$F_e = e^{e\Phi/T_e}F_0 + h, \tag{1}$$

where Φ is the electrostatic potential, F_0 is the equilibrium electron PDF, and h is the nonadiabatic response of the electrons. As is apparent from the above equation, one can expect that by numerically evolving h only, the linear and nonlinear properties of the simulated plasmas will be improved, since the response associated with the electrons that respond adiabatically to the waves has been analytically removed. To make connection with the conventional δf method[32–34,36] one can write Eq. (1) as $F_e = F_0 + \delta f$, where

$$\delta f \equiv (e^{e\Phi/T_e} - 1)F_0 + h. \tag{2}$$

Since the fluctuations are small, $\|e\Phi/T_e\| \ll 1$, one is tempted to expand the right-hand side of Eq. (2) as

$$\delta f \simeq \frac{e\Phi}{T_e}F_0 + h. \tag{3}$$

In the linear regime, the two approaches[11,12] described by Eqs. (2) and (3) are equivalent. In order to systematically remove *all* the terms involving the parallel dynamics in the evolution equation for h, it is preferable to retain the full form given in Eq. (2). However one must now solve a nonlinear Poisson equation; such nonlinear elliptic PDE can be solved iteratively using Newton's method. However, the present gyrokinetic formalism widely used in the magnetic fusion community always assumes that $e\Phi/T_e \ll 1$ and this type of iteration is not necessary. However, at the tokamak edge, the small amplitude assumption may not be valid and a new type of gyrokinetic formalism along with the full Boltzmann response may be needed.

B. Model equations for treating nonadiabatic electrons in toroidal geometry

This section is devoted to the formulation of the scheme of separating the electron adiabatic response from its nonadiabatic counterpart in toroidal geometry, which is essentially a generalization of the methodology presented earlier in Refs. 11 and 12. The main differences are the appearance of terms related to the magnetic field inhomogeneity, the local variation of plasma parameters and the treatment of zonal flows (which are of course absent in a one-dimensional model). In the absence of collisions and in the electrostatic limit, the distribution function for species j is governed by[37–39]

$$\frac{\partial F_j}{\partial t} + \left(v_\parallel(\hat{\mathbf{b}} + \rho_\parallel \hat{\mathbf{b}} \times \boldsymbol{\kappa}) + \frac{\mu}{\omega_{cj}}\hat{\mathbf{b}} \times \boldsymbol{\nabla} B + \mathbf{V}_E \right) \cdot \boldsymbol{\nabla} F_j - (\hat{\mathbf{b}} + \rho_\parallel \hat{\mathbf{b}} \times \boldsymbol{\kappa}) \cdot \left(\mu \boldsymbol{\nabla} B + \frac{q_j}{m_j} \boldsymbol{\nabla} \langle \Phi \rangle_g \right) \frac{\partial F_j}{\partial v_\parallel} = 0, \tag{4}$$

where $\langle \Phi \rangle_g$ is the gyrophase averaged electrostatic potential, $\mathbf{V}_E = c\hat{\mathbf{b}} \times \boldsymbol{\nabla} \langle \Phi \rangle_g / B$ is the $\mathbf{E} \times \mathbf{B}$ drift velocity, $\rho_\parallel = v_\parallel / \omega_{cj}$ is the parallel gyroradius, $\omega_{cj} = (q_j B)/(m_j c)$ is the cyclotron frequency, $\mu = v_\perp^2/(2B)$ is related to the magnetic moment, $\boldsymbol{\kappa} = (\hat{\mathbf{b}} \cdot \boldsymbol{\nabla})\hat{\mathbf{b}}$ is the magnetic curvature and $\hat{\mathbf{b}} = \mathbf{B}/B$ is a unit vector in the direction of the confining magnetic field. For the electrons, the gyrophase averaged potential that appears in Eq. (4) is replaced by the potential evaluated at the particle position itself; the replacement $\langle \Phi \rangle_g \mapsto \Phi$ (for the electrons only!) implies that terms of order $\mathcal{O}(\|\Phi\| k_\perp^2 \rho_e^2)$ and higher are neglected (here $\|\bullet\|$ denotes an appropriate norm). The ion dynamics are modeled using the standard δf scheme,[33,36] which is a Monte Carlo method known as the control variate method.[3] The ion distribution function is written as $F_i = F_{Mi} + \delta f_i$, where F_{Mi} is a Maxwellian with temperature $T_i(r)$ and density $n_0(r)$, and δf_i is a perturbation (assumed to be small); substitution in Eq. (4) then yields an expression for the marker weight $W \equiv \delta f_i / F_i$,

$$\frac{dW}{dt} = (1 - W)\left(\mathbf{V}_E \cdot \mathbf{G}_i - \frac{e}{T_i}\mathbf{V}_{gci} \cdot \boldsymbol{\nabla} \langle \Phi \rangle_g \right), \tag{5}$$

where $\mathbf{G}_i = \boldsymbol{\kappa}_n [1 + \eta_i (\varepsilon / V_{thi}^2 - 3/2)]$, $\boldsymbol{\kappa}_n \equiv -\boldsymbol{\nabla} n_0 / n_0$, $\eta_i \equiv (\boldsymbol{\nabla} T_i / T_i)/(\boldsymbol{\nabla} n_0 / n_0)$, $\varepsilon \equiv v_\parallel^2/2 + \mu B$, and $\mathbf{V}_{gci} = v_\parallel \hat{\mathbf{b}} + \omega_{ci}^{-1} \hat{\mathbf{b}} \times (v_\parallel^2 \boldsymbol{\kappa} + \mu \boldsymbol{\nabla} B) + c \langle \mathbf{E} \rangle_g \times \mathbf{B}/B^2$ is the ion guiding center velocity. The first term on the right-hand side of Eq. (5) represents the tapping of free energy from the ion pressure gradient, whereas the second term accounts for the work of the electric field on the ion guiding center motion. One main goal of this paper is to develop a viable algorithm to treat the electron dynamics. The method presented below is a generalization of the earlier schemes.[11,12] In Ref. 11 a systematic method for treating the electron dynamics was presented for a simple one-dimensional problem; essentially it was suggested to formulate an ansatz for the electron PDF of the form $F_e = \mathcal{H}(\Phi) F_{Me} + h$, where $\mathcal{H}(\Phi)$ is an unknown function and h represents the nonadiabatic response of the electrons. The specific form of the function $\mathcal{H}(\Phi)$ can be found by demanding that all terms involving the parallel velocity disappear. Following Refs. 11 and 18 we can generalize the scheme to general toroidal geometry by writing

$$F_e = \exp[e(\Phi - \langle \Phi \rangle)/T_e] F_{Me} + h, \tag{6}$$

where F_{Me} denotes a Maxwellian with temperature $T_e(r)$ and density $n_0(r)$. Here $\langle \Phi \rangle$ denotes the flux surface average of the electrostatic potential (or zonal flow[28,40])

$$\langle \Phi \rangle \equiv \frac{1}{\sigma(\psi)} \int_0^{2\pi} d\zeta \int_0^{2\pi} \mathcal{J} \Phi \, d\theta, \tag{7}$$

where

$$\sigma(\psi) \equiv \int_0^{2\pi} d\zeta \int_0^{2\pi} \mathcal{J} d\theta.$$

Here $\mathcal{J} \equiv [\nabla\psi \cdot (\nabla\theta \times \nabla\zeta)]^{-1}$ is the Jacobian of the transformation from the magnetic coordinates $\{\psi, \theta, \zeta\}$ to the Cartesian coordinates. As before h represents the nonadiabatic electron response. The dynamics of the nonadiabatic part of the electron distribution function is obtained by substituting Eq. (6) in $dF_e/dt=0$, which can be also be written in terms of the weight $\mathcal{W} \equiv h/F_e$,

$$\frac{d\mathcal{W}}{dt} = (1-\mathcal{W})\left(\mathbf{G}_e \cdot \mathbf{V}_E - \chi + \mathbf{V}_{de} \cdot \frac{e}{T_e} \nabla \langle \Phi \rangle\right), \tag{8}$$

where $\mathbf{G}_e = \boldsymbol{\kappa}_n (1 + \eta_e (\varepsilon / V_{the}^2 - 3/2))$, $\mathbf{V}_{de} = \omega_{ce}^{-1} \hat{\mathbf{b}} \times (v_\parallel^2 \boldsymbol{\kappa} + \mu \nabla B)$ is the curvature drift velocity for the electrons, and $V_{the} = \sqrt{T_e/m_e}$. By construction[11], and unlike the conventional δf scheme, there is no contribution from the free streaming of the electrons along the magnetic field lines. As in the one-dimensional version of the scheme[11,12], one must determine the so-called scalar polarization field,[11] $\chi \equiv (e/T_e)\partial\Phi/\partial t$. In addition, we must also determine the electrostatic potential itself. For this purpose we employ the gyrokinetic Poisson equation[15,16]

$$\frac{\tau}{\lambda_D^2}(\Phi - \tilde{\tilde{\Phi}}) = 4\pi e(\delta\bar{n}_i - \delta n_e), \tag{9}$$

where

$$\tilde{\tilde{\Phi}}(\mathbf{x}) = \frac{1}{2\pi n_0} \int \langle \Phi \rangle_g (\mathbf{R}) F_{Mi}(\mathbf{R}, \mu, v_\parallel) \times \delta(\mathbf{R} - \mathbf{x} + \boldsymbol{\rho}) d\mathbf{R} d\mathbf{v} d\varphi, \tag{10}$$

$$\langle \Phi \rangle_g (\mathbf{R}) = \frac{1}{2\pi} \int \Phi \, \delta(\mathbf{x} - \mathbf{R} - \boldsymbol{\rho}) d\mathbf{x} d\varphi, \tag{11}$$

and δn_e is the perturbed part of the electron density response of $\int F d\mathbf{v}$, and F is given by Eq. (6). Therefore, Eq. (9) becomes a nonlinear equation. However, people in the fusion community, by following the gyrokinetic ordering, generally solve the linearized version of the equation by assuming that $e\Phi/T_e$ is small. Therefore, the existing Poisson solver in GTC (Ref. 28) can be readily used for our purpose. Here $\mathbf{x}$ and $\mathbf{R}$ are the particle and guiding center positions, respectively; $\boldsymbol{\rho}$ is the gyroradius vector with magnitude $\rho = v_\perp/\omega_{ci}$, φ is the local gyrophase, τ is the electron-to-ion temperature ratio, and λ_D is the plasma Debye length. The electrostatic potential [Eq. (9)] is obtained by using a generalized gyrokinetic Poisson solver[27,28] that is based on the physical process of gyrophase averaging in configuration space (rather than in Fourier space). In order to determine χ that appears in the weight equation for the electrons, we proceed as in the one-dimensional case[11,12] by operating with $\partial/\partial t$ on the gyrokinetic Poisson Eq. (9), and by taking the appropriate velocity moment of the Vlasov equation, Eq. (4). However, in contrast to the one-dimensional case, one must pay special attention to the curvature and the finite Larmor radius (FLR) effects; in the limit of $|k_\perp \rho_i| \leqslant 2$, with $\tilde{\tilde{\chi}} = I_0(b) e^{-b} \chi \simeq (1 - \rho_i^2 \nabla_\perp^2)^{-1} \chi$, the procedure outlined above yield

$$n_0 \tau \rho_i^2 \nabla_\perp^2 \chi = (1 - \rho_i^2 \nabla_\perp^2) \nabla \cdot \boldsymbol{\Gamma}, \tag{12}$$

where $\boldsymbol{\Gamma} = \boldsymbol{\Gamma}_{\rm gc} + \boldsymbol{\Gamma}_{\rm FLR}$,

$$\boldsymbol{\Gamma}_{\rm gc} \equiv \int (\hat{\mathbf{b}} v_\parallel + \mathbf{V}_E + \mathbf{V}_{de}) h d\mathbf{v} + \frac{e}{T_e}(\Phi - \langle \Phi \rangle) \times \int \mathbf{V}_{de} F_{Me} d\mathbf{v} - \frac{1}{2\pi} \times \int \left(v_\parallel \hat{\mathbf{b}} + \frac{c}{B^2} \langle \mathbf{E} \rangle_g \times \mathbf{B} + \mathbf{V}_{di} \right) \times \delta f_i \delta(\mathbf{R} - \mathbf{x} + \boldsymbol{\rho}) d\mathbf{R} d\mathbf{v} d\varphi, \tag{13}$$

and

$$\boldsymbol{\Gamma}_{\rm FLR} \equiv c \int F_{Me} \frac{\mathbf{E} \times \mathbf{B}}{B^2} d\mathbf{v} - \frac{c}{2\pi} \int F_{Mi} \frac{\langle \mathbf{E} \rangle_g \times \mathbf{B}}{B^2} \delta(\mathbf{R} - \mathbf{x} + \boldsymbol{\rho}) d\mathbf{R} d\mathbf{v} d\varphi. \tag{14}$$

Here $\mathbf{V}_{dj} \equiv \omega_{cj}^{-1} \hat{\mathbf{b}} \times (v_\parallel^2 \boldsymbol{\kappa} + \mu \nabla B)$ is the curvature drift velocity for particle species j and $\langle \mathbf{E} \rangle_g$ is the local gyrophase averaged electric field. The contribution $\boldsymbol{\Gamma}_{\rm FLR}$ arises due to the fact that the ion Larmor gyroradius is finite. Equation (12) cannot be solved with the Poisson solver in GTC. Instead, we have used the latest finite-element interface developed by Nishimura *et al.*[17] to link GTC with PESTc (Ref. 35) for solving Eq. (12). Note that the first term on the right-hand side of Eq. (13), which is related to the electron flux along the magnetic field lines, dominates over the remaining terms; the parallel electron flux, however, *does not* contribute to the zonal component of χ and other terms are important as far as the computation of $\langle \chi \rangle$ is concerned. To show this, we consider the case of a plasma with circular (or nearly circular) magnetic surfaces. As shown in the Appendix, Eq. (12) can be used to approximately calculate the zonal component of the polarization field

$$n_0 \tau \langle \rho_i^2 \rangle \frac{d}{d\psi} \left(\langle g^{\psi\psi} \rangle \frac{d}{d\psi} (\sigma \langle \chi \rangle) \right) + n_0 \tau \langle \rho_i^2 \rangle \frac{1}{\sigma} \frac{d}{d\psi} (\sigma \langle \sqrt{g^{\psi\psi}} \kappa_N \rangle \langle \chi \rangle) = -\frac{d}{d\psi} (\sigma \langle \Gamma^\psi \rangle),$$

where $\Gamma^\psi = \nabla\psi \cdot \boldsymbol{\Gamma}$, κ_N is the normal component of the magnetic curvature, and $g^{\psi\psi} = \nabla\psi \cdot \nabla\psi$ is a metric element. Considering the right-hand side of the above equation we clearly see that the parallel electron flux term in Eq. (13) does not contribute to the radial flux Γ^ψ since, for a plasma with nested magnetic surfaces, $\mathbf{B} \cdot \nabla\psi \equiv 0$. In summary the computational procedure for treating the nonadiabatic response of the electrons in toroidal geometry is as follows: time advancing Eqs. (5) and (8) for the ion weight, $W = \delta f_i / F_i$, and the electron weight, $\mathcal{W} = h/F_e$ (which is associated with the nonadiabatic electron response), one can compute the right-hand side of the gyrokinetic Poisson equation (9) and solve

this integral equation for the electrostatic potential Φ [note that the electron density perturbation contains a nonlinear term in the electrostatic potential; taking into account that $e(\Phi-\langle\Phi\rangle)/T_e \ll 1$, at least in the plasma core, this term can be solved iteratively, or simply linearized as done in Ref. 18]; then determines the fluxes given by Eqs. (13) and (14) and inverts Eq. (12) to obtain the polarization field χ. It is worth noting that the equation for the electron weight $\mathcal{W}$ requires both scalar fields Φ and χ, whereas the equation governing the ion weight W depends on the electrostatic potential Φ alone.

III. LINEAR BENCHMARKS AND PRELIMINARY NONLINEAR RESULTS

In this section, the numerical method for the nonadiabatic electron response in toroidal geometry and its implementation in the global toroidal code (GTC) (Refs. 18 and 41) are briefly discussed. As has been described in the previous section the scheme requires the global (toroidal) solution of an elliptic equation (12) for the new scalar field, $\partial\Phi/\partial t$. The extension of the scheme to finite β gyrokinetic plasmas would also require the solution of such global elliptic equations in toroidal geometry. Therefore, it is crucial to develop an efficient elliptic solver for inverting equations of the form $\nabla_\perp^2\Phi=S$, where S is a known "source term." As mentioned earlier, a finite difference formulation of the perpendicular Laplacian ($\nabla_\perp^2$) and its approximate inverse, $\Phi=\nabla_\perp^{-2}S$, is a nontrivial exercise since the GTC code uses a field-aligned mesh for computational efficiency. The consequence of using the field line following coordinates[19,42] is that the (discrete) computational mesh on a given poloidal plane displays an amount of "twisting" that reflects the shear in the confining magnetic field **B**. Given the structure of the computational mesh, it is best to use the finite element method (FEM). In this paper, we have used the FEM with triangular elements; as a result the original elliptic problem can be cast in matrix form as $\mathbf{A}\cdot\mathbf{\Phi}=\mathbf{S}$, where $\mathbf{\Phi}$ and $\mathbf{S}$ are column vectors and $\mathbf{A}$ denotes the sparse matrix containing the geometric information pertaining to the perpendicular Laplacian. The solution, $\mathbf{\Phi}=\mathbf{A}^{-1}\cdot\mathbf{S}$, is computed using the scalable routines of PETSc (Portable, Extensible Toolkit for Scientific Computation).[35] The Poisson solver for the inversion of the elliptic PDE $\nabla_\perp^2\Phi=S$ has been successfully implemented in the GTC code and the details of the implementation have recently been reported.[17]

As just mentioned, the global gyrokinetic code GTC is based on a computational mesh in configuration space that is approximately aligned with the pitch of the magnetic field line. For the strongly anisotropic modes ($k_\parallel/k_\perp \ll 1$) that characterize the ITG turbulence, this results in a considerable improvement in the overall computational efficiency. The consequence of using a field aligned mesh is that the FEM decomposition is unique to a given poloidal plane. Following Nishimura *et al.*,[17] Fig. 1 shows a typical FEM grid, based on triangular elements, on a specific poloidal plane with 4608 triangular elements corresponding to 2400 vertices. Note that the low-resolution grid of Fig. 1 is used for illustrative purposes only, and the actual FEM grid used in the turbulence simulations covers most of the radial domain and possesses a much higher resolution.

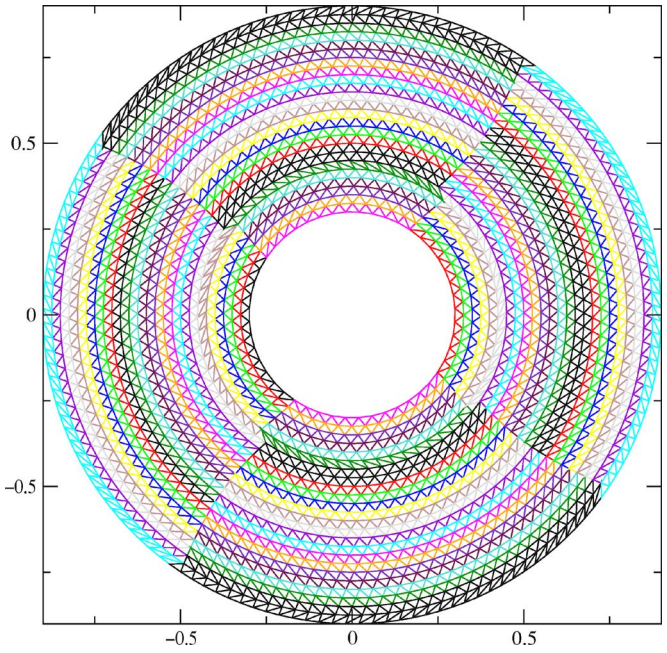

FIG. 1. Low-resolution finite-element (FEM) grid for one poloidal plane. The FEM grid has 2400 vertices (or nodes) and 4608 elements. In practice the FEM grid actually used in turbulence simulations has a much higher resolution with 41 280 vertices and 81 920 elements covering the radial domain $r/a=[0.1,0.9]$.

The present toroidal scheme has been benchmarked against the numerical results[14] obtained from the FULL code which is comprehensive one-dimensional (radially local) eigenvalue code described in Refs. 43 and 44, and references therein. The local parameters for the linear benchmark are[45,46] $q=1.4$ (at $r/a=0.5$), $R_0/L_n=2.2$, $R_0/L_{Te}=6.92$, global magnetic shear parameter $\hat{s}=r(dq/dr)/q=0.78$ (at $r/a=0.5$), inverse aspect ratio $\epsilon=a/R_0=0.358$ (here R_0 is the major radius, L_n is the density scale length, L_{T_e} is the electron temperature scale length, and a is the minor radius). The safety factor is of the form $q=q_0+q_1(r/a)+q_2(r/a)^2$ with parameters $(q_0,q_1,q_2)=(0.854,0.000,2.184)$. The local parameters for the linear benchmark are the same as the earlier benchmark between the FULL code, the GTC code using the fluid-kinetic hybrid electron model,[18] and the three-dimensional global gyrokinetic GT3D code.[29]

The linear benchmarks and the nonlinear simulations presented in this paper have been carried out in a computational domain with radial width $r/a\in[0.1,0.9]$ (the radial width of the computational domain is about 125 thermal ion gyroradii across); the corresponding FEM grid has 81 920 triangular elements and 41 280 vertices. Figure 2 shows the linear growth rate as a function of the ion temperature gradient parameter $\eta_i\equiv L_{T_i}/L_n$ for a fixed value of $k_\theta\rho_i=0.336$ (at $r/a=0.5$). The dashed line is the trapped electron mode (TEM) branch obtained using the FULL code, whereas the dotted line represents the ITG branch, both at $r/a=0.5$. The plain line shows the linear growth rate computed using the toroidal splitting scheme; the overall agreement is good except perhaps for larger values of η_i. Figure 3 shows the real

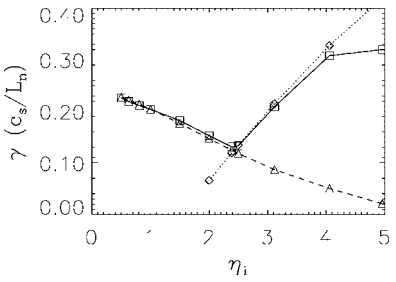

FIG. 2. Linear growth rate as a function of the ion temperature gradient parameter $\eta_i = L_n/L_{Ti}$ using the splitting scheme (plain line; squares) for a fixed value of $k_\theta \rho_i = 0.336$. The linear growth rates associated with the TEM branch (dashed line; triangles) and the ITG branch (dotted line; diamonds) as computed using the FULL code are also shown.

part of the mode frequency for the same parameters as in Fig. 2. For small η_i the mode rotates in the electron diamagnetic direction $\omega_r > 0$; as the ion temperature gradient parameter is increased the mode rotation reverses to the ion diamagnetic direction. The plain line shows the results obtained using the splitting scheme. Note that the method to compute the polarization field, $\chi \propto \partial\Phi/\partial t$, is not unique; in fact it is possible to use time-centered differences to evaluate $\partial\Phi/\partial t$. The dotted line shows the results obtained based on the time-centered differencing technique for the polarization field. The good agreement between the two methods actually highlights the efficiency of the present scheme (6) for electron dynamics. The dashed lines in Fig. 3 are those obtained using the FULL code. These results are in good agreement with the results presented in Ref. 18.

Nonlinear global simulations of ITG turbulence in the presence of kinetic electrons were carried out using the same parameters as those of Figs. 2 and 3 (in addition $R_0/L_{T_i} = 6.92$). The turbulent radial heat flux Q averaged over a radial annulus of volume V

$$Q \equiv \frac{1}{V}\int m_i \varepsilon \mathbf{n}\cdot c\frac{\langle \mathbf{E}\rangle_g \times \mathbf{B}}{B^2} F_i d\mathbf{R} d\mathbf{v},$$

is used to determine the ion heat diffusivity coefficient $\chi_i = -Q/(dp_{i0}/dr)$; here $\varepsilon \equiv v_\parallel^2/2 + \mu B$ is the kinetic energy per unit mass, $\mathbf{n} = \nabla\psi/\sqrt{g^{\psi\psi}}$ is a unit vector normal to a magnetic surface and pointing outwards. Figure 4 shows the time evolution of the ion heat diffusivity coefficient for a simulation with $N_c^{(e)} = 8$ electron markers and $N_c^{(i)} = 8$ ion markers per computational cell. The dotted lines show the range of χ_i values at $c_s t/a = 360$ for various adiabatic runs with the same local parameters and the same number of ion markers; the multiple adiabatic runs were carried out by slightly altering the initial location of the ion markers in phase space. From Fig. 4 we can infer that the ion heat diffusivity in the presence of kinetic electrons is about 2 to 3 times larger as compared to the case with adiabatic electrons. Figure 5 shows the instantaneous sheared flow (normalized to the ion sound speed $c_s = \sqrt{T_e/m_i}$) at $c_s t/a = 360$ for the same simulation and physical parameters as in Fig. 4. The amplitude of the sheared flow in the presence of kinetic electrons is comparable to that obtained with adiabatic electrons. However, in contrast to the adiabatic case, the radial structure of the sheared flow has additional features with much shorter wavelength. In particular, simulations with kinetic electrons have shown that sheared flows with (radial) wavelengths $\lambda_r \sim \sqrt{a\rho_i}$ are always present. There are significant differences between the fully kinetic and adiabatic cases; (a) the time evolution of the ion heat diffusivity in the presence of trapped electrons does not show the presence of significant secondary or tertiary peaks as in the adiabatic case; (b) the $\mathbf{E}\times\mathbf{B}$ sheared flow has a much finer radial structure in the presence of trapped electrons; these effects (a) and (b) are actually related, but this aspect will be addressed in more detail in a future publication.

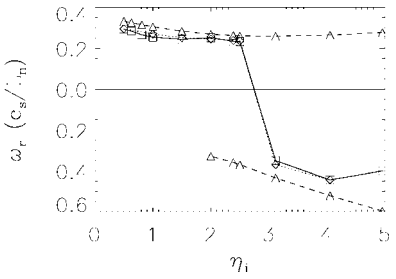

FIG. 3. Mode frequency as a function of the ion temperature gradient parameter $\eta_i = L_n/L_{Ti}$ using the splitting scheme (plain line; squares) and the hybrid scheme (dotted line; diamonds). The mode frequency associated with the TEM branch (dashed line; upper curve) and the ITG branch (dashed line; lower curve) as computed using the FULL code are also shown.

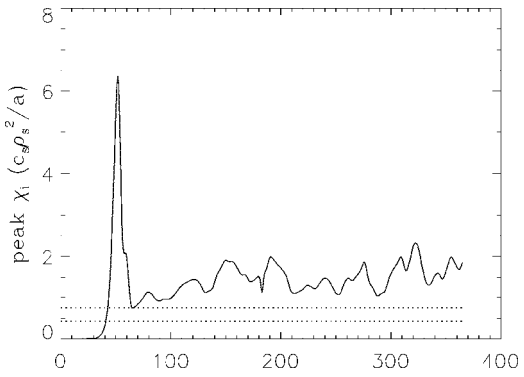

FIG. 4. Peak ion diffusivity coefficient as a function of time for simulations with $N_c = 8$ ions and electrons per cell. The radial extent of the simulated plasma is equivalent to 125 thermal gyroradii. The horizontal curves show the range of χ_i values at $tc_s/a = 360$ in the adiabatic limit for various initial conditions.

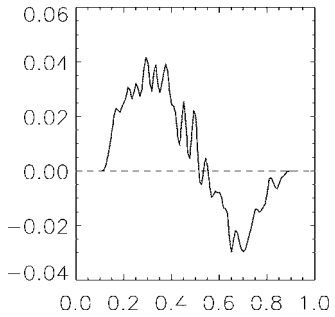

FIG. 5. Shear flow at $c_s t/a = 360$ (fully developed turbulent regime) in the presence of trapped electrons for the same parameters as in Fig. 4.

IV. CONCLUSIONS

The efficient numerical scheme which splits the adiabatic electrons from the nonadiabatic electrons has been successfully implemented in a global toroidal code. Linear benchmarks with the FULL code[43,44] show reasonable agreement with the global, initial-value code. For a medium sized plasma (minor radius $a=125\rho_i$, where ρ_i is the ion thermal gyroradius), the ion heat transport in the presence of kinetic electrons increases by a factor 2–3 compared with the adiabatic case. In addition, the $\mathbf{E}\times\mathbf{B}$ sheared flow has a shorter radial structure for the case with trapped electrons. This paper is part of ongoing work, and further simulations are required to understand the properties of the ITG turbulence in the presence of magnetically trapped electrons.

ACKNOWLEDGMENTS

One of the authors (J.L.V.L.) would like to acknowledge useful and constructive discussions with Professor Jan Weiland.

This research was supported by Contract No. DE-AC02-CH0-3073 and the Scientific Discovery through Advanced Computing (SciDAC) initiative (U.S. Department of Energy).

APPENDIX: ESTIMATE OF ZONAL FLOW ASSOCIATED WITH THE POLARIZATION FIELD

The equation governing the polarization field $\chi\equiv\partial\Phi/\partial t$ is

$$n_0\tau(\chi-\tilde{\tilde{\chi}})=\boldsymbol{\nabla}\cdot\boldsymbol{\Gamma}, \tag{A1}$$

where

$$\tilde{\tilde{\chi}}=\frac{1}{2\pi n_0}\int\langle\chi\rangle_g F_{Mi}\delta(\mathbf{R}-\mathbf{x}+\boldsymbol{\rho})d\mathbf{R}d\mathbf{v}d\varphi. \tag{A2}$$

For the remainder of this Appendix it is convenient to introduce a set of useful definitions. Consider an arbitrary function $F=F(\psi,\theta,\zeta)$ specified in terms of the magnetic coordinates $\{\psi,\theta,\zeta\}$; the Jacobian of the transformation from the magnetic coordinates to the Cartesian coordinates is denoted $\mathcal{J}\equiv[\boldsymbol{\nabla}\psi\cdot(\boldsymbol{\nabla}\theta\times\boldsymbol{\nabla}\zeta)]^{-1}$. The flux-surface average of F is defined as

$$\langle F\rangle\equiv\frac{1}{\sigma}\int_0^{2\pi}d\zeta\int_0^{2\pi}F\mathcal{J}d\theta, \tag{A3}$$

where

$$\sigma(\psi)\equiv\int_0^{2\pi}d\zeta\int_0^{2\pi}\mathcal{J}d\theta, \tag{A4}$$

whereas the volume average of F is

$$\bar{F}\equiv\frac{\int_0^{\psi_b}\sigma(\psi)\langle F\rangle d\psi}{\int_0^{\psi_b}\sigma(\psi)d\psi}. \tag{A5}$$

Here ψ_b is the toroidal flux function evaluated at the plasma boundary. Given the fact that the function F is periodic in the poloidal and toroidal angles it follows that

$$\left\langle\frac{\partial F}{\partial\theta}\right\rangle=\left\langle\frac{\partial F}{\partial\zeta}\right\rangle=0, \tag{A6}$$

and

$$\left\langle\frac{\partial F}{\partial\psi}\right\rangle=\frac{1}{\sigma}\frac{d}{d\psi}(\sigma\langle F\rangle). \tag{A7}$$

A direct consequence of Eqs. (A6) and (A7) is that the flux-surface average of the divergence of an arbitrary vector field $\mathbf{A}$ assumes the simple form of

$$\langle\boldsymbol{\nabla}\cdot\mathbf{A}\rangle=\left\langle\frac{1}{\mathcal{J}}\left(\frac{\partial}{\partial\psi}(\mathcal{J}A^{\psi})+\frac{\partial}{\partial\theta}(\mathcal{J}A^{\theta})+\frac{\partial}{\partial\zeta}(\mathcal{J}A^{\zeta})\right)\right\rangle$$
$$=\frac{1}{\sigma}\frac{d}{d\psi}(\sigma A^{\psi}), \tag{A8}$$

where $A^{\eta}\equiv\mathbf{A}\cdot\boldsymbol{\nabla}\eta$ for $\eta=(\psi,\theta,\zeta)$. Assuming that the polarization field χ can be written as a linear superposition of plane waves (a better approach would be to use the Fourier-Bessel representation as suggested in Ref. 47 although the lowest-order expression for the zonal component $\langle\chi\rangle$ remains unaffected) one notes that $\tilde{\tilde{\chi}}=\Gamma_0(b)\chi$ where $b=k_\perp^2\rho_i^2$; here $\Gamma_0(x)=e^{-x}I_0(x)$ and $I_0(x)$ is the modified Bessel function of order zero with argument x. Writing the Taylor expansion of Γ_0 as

$$\Gamma_0(b)=1-b+\sum_{k=2}^{\infty}\alpha_k b^k, \tag{A9}$$

and using the transformation of $b\mapsto-\rho_i^2\nabla_\perp^2$ from Fourier space to real space, one obtains

$$\tilde{\tilde{\chi}}=\left[I+\rho_i^2\nabla_\perp^2+\sum_{k=2}^{\infty}(-1)^k\alpha_k\rho_i^{2k}\nabla_\perp^{2k}\right]\chi, \tag{A10}$$

where I is the identity operator. If k_{zf} denotes the magnitude of the (radial) wave vector of the zonal component of χ and if $k_\perp$ denotes the typical magnitude of the wave vector associated with $\chi-\langle\chi\rangle$ we note that $k_{\mathrm{zf}}^2\rho_i^2\ll k_\perp^2\rho_i^2\ll 1$. Therefore, to a very good approximation, we can neglect the last term in the square brackets in Eq. (A10). It follows that

$$\langle\tilde{\tilde{\chi}}\rangle\simeq\langle\chi\rangle+\langle\rho_i^2\nabla_\perp^2\chi\rangle\simeq\langle\chi\rangle+\langle\rho_i^2\rangle\langle\nabla_\perp^2\chi\rangle. \tag{A11}$$

The last expression in the above equation can be justified as follows. If $L_{T_i}=|\boldsymbol{\nabla}T_i/T_i|^{-1}$ is the scale length associated with the ion temperature profile and $L_B=|\boldsymbol{\nabla}B/B|^{-1}$ is the scale length of the magnetic field, and noting that $\rho_i^2\propto T_i(\psi)/B^2$, it follows that $\rho_i^2=\langle\rho_i^2\rangle+\mathcal{O}(\overline{\rho_i^2}L_{T_i}/L_B)\simeq\langle\rho_i^2\rangle$ (this approximation breaks down for a flat ion temperature profile for which L_{T_i}/L_B can be of order unity or larger). The last step of the

derivation involves the property of $\langle Fg(\psi)\rangle = g(\psi)\langle F\rangle$ for an arbitrary flux-surface quantity $g(\psi)$. In order to proceed further we must derive the explicit form of the perpendicular Laplacian in toroidal geometry. First the perpendicular gradient of F can be defined formally in operator form as $\nabla_\perp \equiv (\mathbf{I} - \hat{\mathbf{b}}\hat{\mathbf{b}}) \cdot \nabla$ (where $\hat{\mathbf{b}} = \mathbf{B}/B$ is a unit vector along the magnetic field direction and $\mathbf{I}$ is the unit tensor), or in explicit (and more practical) form as

$$\nabla_\perp F = \nabla F - \hat{\mathbf{b}} \frac{\partial F}{\partial \ell}, \tag{A12}$$

where $\partial F/\partial \ell \equiv \hat{\mathbf{b}} \cdot \nabla F$ (the coordinate ℓ is related to the distance along a given magnetic field line). Operating with $\nabla_\perp$ on both sides of Eq. (A12) yields the relation

$$\nabla_\perp^2 F = \nabla \cdot \nabla_\perp F + \boldsymbol{\kappa} \cdot \nabla F = \nabla^2 F - \frac{\partial^2 F}{\partial \ell^2} - \nabla \cdot \hat{\mathbf{b}} \frac{\partial F}{\partial \ell} + \boldsymbol{\kappa} \cdot \nabla F, \tag{A13}$$

where $\boldsymbol{\kappa} = \partial \hat{\mathbf{b}}/\partial \ell$ is the magnetic curvature. Using Eqs. (A8) and (A12) we obtain

$$\langle \nabla_\perp^2 F \rangle \simeq \frac{1}{\sigma} \frac{d}{d\psi} \left(\langle g^{\psi\psi} \rangle \frac{d}{d\psi} (\sigma \langle F \rangle) \right) + \frac{1}{\sigma} \frac{d}{d\psi} (\sigma \langle \sqrt{g^{\psi\psi}} \kappa_N \rangle \times \langle F \rangle), \tag{A14}$$

where $\kappa_N = \hat{\mathbf{n}} \cdot \boldsymbol{\kappa}$ is the normal component of the magnetic curvature; here $\hat{\mathbf{n}} = \nabla\psi/\sqrt{g^{\psi\psi}}$ is a unit vector orthogonal to $\mathbf{B}$ and normal to the magnetic surface $\psi = \text{const}$. In deriving Eq. (A14) we have also made use of the fact that the shape of the magnetic surfaces do not depart strongly from circularity, that is

$$\langle (g^{\bar{\psi}\bar{\psi}})^2 \rangle^{1/2} \gg \langle (g^{\bar{\psi}\theta})^2 \rangle^{1/2}; \langle (g^{\bar{\psi}\zeta})^2 \rangle^{1/2}, \tag{A15}$$

where $\bar{\psi} \equiv \psi/\psi_b \in [0,1]$ is the normalized toroidal flux function. Combining Eqs. (A1), (A10), and (A14), and again using the relation (A8), we arrive at the following estimate for the zonal component of the polarization field $\chi = \partial\Phi/\partial t$,

$$n_0 \tau \langle \rho_i^2 \rangle \frac{d}{d\psi} \left(\langle g^{\psi\psi} \rangle \frac{d}{d\psi} (\sigma \langle \chi \rangle) \right) + n_0 \tau \langle \rho_i^2 \rangle \frac{1}{\sigma} \frac{d}{d\psi} (\sigma \langle \sqrt{g^{\psi\psi}} \kappa_N \rangle \langle \chi \rangle) = -\frac{d}{d\psi} (\sigma \langle \Gamma^\psi \rangle),$$

where $\Gamma^\psi = \nabla\psi \cdot \boldsymbol{\Gamma}$.

[1] P. C. Liewer, Nucl. Fusion **25**, 543 (1985).
[2] F. Wagner and U. Stroth, Plasma Phys. Controlled Fusion **35**, 1321 (1993).
[3] J. M. Hammerseley and D. C. Handscomb, *Monte Carlo Methods* (Chapman and Hall, London, 1965).
[4] J. L. V. Lewandowski, Phys. Lett. A **313**, 291 (2003).
[5] J. J. Hopfield, Proc. Natl. Acad. Sci. U.S.A. **79**, 2554 (1982).
[6] J. J. Hopfield and D. W. Tank, Biol. Cybern. **52**, 141 (1985).
[7] C. Koch, J. Marroquin, and A. Yulle, Proc. Natl. Acad. Sci. U.S.A. **83**, 4263 (1986).
[8] J. L. V. Lewandowski, Phys. Plasmas **12**, 052322 (2005).
[9] W. Horton, *Handbook of Plasma Physics* (Elsevier, Amsterdam, 1984), Vol. 2.
[10] W. Horton, Rev. Mod. Phys. **71**, 735 (1999).
[11] J. L. V. Lewandowski, Phys. Plasmas **10**, 3204 (2003).
[12] I. Manuilskiy and W. W. Lee, Phys. Plasmas **7**, 1381 (2000).
[13] J. L. V. Lewandowski, Plasma Phys. Controlled Fusion **45**, L39 (2003).
[14] G. Rewoldt, Z. Lin, and Y. Idomura, Bull. Am. Phys. Soc. **48**, 219 (2003).
[15] W. W. Lee, J. Comput. Phys. **72**, 243 (1987).
[16] W. W. Lee, Phys. Fluids **26**, 556 (1983).
[17] Y. Nishimura, Z. Lin, J. L. V. Lewandowski, and S. Ethier, J. Comput. Phys. **214**, 657 (2006).
[18] Z. Lin, L. Chen, Y. Nishimura, H. Qu, T. S. Hahm, J. L. V. Lewandowski, G. Rewoldt, W. X. Wang, P. H. Diamond, C. Holland, F. Zonca, and Y. Li, in Proceedings of the 20th IAEA Fusion Energy Conference, Vilamoura, Portugal, 1–6 November 2004, IAEA-CN/TH/8-4.
[19] B. Scott, Phys. Plasmas **5**, 2334 (1998).
[20] Y. Chen and S. Parker, Phys. Plasmas **8**, 441 (2001).
[21] Y. Chen and S. Parker, J. Comput. Phys. **189**, 463 (2003).
[22] Z. Lin and L. Chen, Phys. Plasmas **8**, 1447 (2001).
[23] Y. Chen, S. E. Parker, B. I. Cohen, A. Dimits, W. Nevins, D. Shumaker, V. Decyk, and J. Leboeuf, Nucl. Fusion **43**, 1121 (2003).
[24] S. Parker, Y. Chen, W. Wan, B. Cohen, and W. Nevins, Phys. Plasmas **11**, 2594 (2004).
[25] B. Cohen, A. Dimits, W. Nevins, Y. Chen, and S. Parker, Phys. Plasmas **9**, 251 (2002).
[26] B. Cohen, A. Dimits, W. Nevins, Y. Chen, and S. Parker, Phys. Plasmas **9**, 1915 (2002).
[27] Z. Lin and W. W. Lee, Phys. Rev. E **52**, 5646 (1995).
[28] Z. Lin, T. S. Hahm, W. W. Lee, W. M. Tang, and R. B. White, Science **281**, 1835 (1998).
[29] Y. Idomura, S. Tokuda, and Y. Kishimoto, Nucl. Fusion **43**, 234 (2003).
[30] W. W. Lee, J. L. V. Lewandowski, T. S. Hahm, and Z. Lin, Phys. Plasmas **8**, 4435 (2001).
[31] J. L. V. Lewandowski, Comput. Phys. Commun. **164**, 114 (2004).
[32] A. Y. Aydemir, Phys. Plasmas **1**, 822 (1994).
[33] S. Parker and W. W. Lee, Phys. Fluids B **5**, 77 (1993).
[34] R. E. Denton and M. Kotschenreuther, J. Comp. Physiol. **119**, 283 (1995).
[35] PETSc: Portable, Extensive Toolkit for Scientific Computationa Mathematics and Computer Science Division, Argonne National Laboratoty. Available at http://www-unix.mcs.anl.gov/petsc/petsc-2
[36] G. Hu and J. A. Krommes, Phys. Plasmas **1**, 863 (1994).
[37] J. L. V. Lewandowski, "Drift wave models for three-dimensional plasmas," Ph.D. thesis, The Australian National University (1997).
[38] J. L. V. Lewandowski, Phys. Plasmas **7**, 3360 (2000).
[39] T. S. Hahm, Phys. Fluids **31**, 2670 (1988).
[40] A. Hasegawa, C. G. Maclennan, and Y. Kodama, Phys. Fluids **22**, 2122 (1979).
[41] Z. Lin, T. S. Hahm, W. M. Tang, and R. B. White, Phys. Plasmas **7**, 1857 (2000).
[42] A. M. Dimits, Phys. Rev. E **48**, 4070 (1993).
[43] G. Rewoldt, W. M. Tang, and M. S. Chance, Phys. Fluids **25**, 480 (1982).
[44] G. Rewoldt, W. M. Tang, and R. J. Hastie, Phys. Fluids **30**, 807 (1987).
[45] A. M. Dimits, G. Bateman, M. A. Beer *et al.*, Phys. Plasmas **7**, 969 (2000).
[46] J. L. V. Lewandowski, J. Comput. Methods Sci. Eng., **6**, 271 (2005).
[47] J. L. V. Lewandowski, Z. Lin, W. W. Lee, and T. S. Hahm, Phys. Plasmas **7**, 588 (2000).